J|A|C|S
ARTICLES

Published on Web 12/04/2008

Sequence-Scrambling Fragmentation Pathways of Protonated Peptides

Christian Bleiholder,[†] Sandra Osburn,[‡] Todd D. Williams,[§] Sándor Suhai,[†] Michael Van Stipdonk,*[,‡] Alex G. Harrison,*[,||] and Béla Paizs*[,†]

Department of Molecular Biophysics, Im Neuenheimer Feld 580, German Cancer Research Center, 69120 Heidelberg, Germany, Department of Chemistry, Wichita State University, Wichita, Kansas 67260, Molecular Structures Group, Department of Chemistry, University of Kansas, Lawrence, Kansas 66045, and Department of Chemistry, University of Toronto, 80 St. George Street, Toronto, Ontario M5S 3H6, Canada

Received July 2, 2008; E-mail: Mike.VanStipdonk@Wichita.edu; aharriso@chem.utoronto.ca; B.Paizs@dkfz.de

Abstract: The gas-phase structures and fragmentation pathways of the N-terminal *b* and *a* fragments of YAGFL-NH_2, AGLFY-NH_2, GFLYA-NH_2, FLYAG-NH_2, and LYAGF-NH_2 were investigated using collision-induced dissociation (CID) and detailed molecular mechanics and density functional theory (DFT) calculations. Our combined experimental and theoretical approach allows probing of the scrambling and rearrangement reactions that take place in CID of *b* and *a* ions. It is shown that low-energy CID of the b_5 fragments of the above peptides produces nearly the same dissociation patterns. Furthermore, CID of protonated *cyclo*-(YAGFL) generates the same fragments with nearly identical ion abundances when similar experimental conditions are applied. This suggests that rapid cyclization of the primarily linear b_5 ions takes place and that the CID spectrum is indeed determined by the fragmentation behavior of the cyclic isomer. This can open up at various amide bonds, and its fragmentation behavior can be understood only by assuming a multitude of fragmenting linear structures. Our computational results fully support this cyclization−reopening mechanism by showing that protonated *cyclo*-(YAGFL) is energetically favored over the linear b_5 isomers. Furthermore, the cyclization−reopening transition structures are energetically less demanding than those of conventional bond-breaking reactions, allowing fast interconversion among the cyclic and linear isomers. This chemistry can lead in principle to complete loss of sequence information upon CID, as documented for the b_5 ion of FLYAG-NH_2. CID of the a_5 ions of the above peptides produces fragment ion distributions that can be explained by assuming *b*-type scrambling of their parent population and $a \rightarrow a^*$-type rearrangement pathways (Vachet, R. W.; Bishop, B. M.; Erickson, B. W.; Glish, G. L. *J. Am. Chem. Soc.* **1997**, *119*, 5481). While *a* ions easily undergo cyclization, the resulting macrocycle predominantly reopens to regenerate the original linear structure. Computational data indicate that the $a \rightarrow a^*$-type rearrangement pathways of the linear *a* isomers involve post-cleavage proton-bound dimer intermediates in which the fragments reassociate and the originally C-terminal fragment is transferred to the N-terminus.

Introduction

Protein identification in proteomics is mainly based on tandem mass spectrometry (MS/MS) analysis of peptides[1] that are produced by enzymatic digestion of protein mixtures. In the most common MS/MS experiments, protonated peptides are collisionally excited to induce dissociation and the fragment-ion spectrum is used to decipher peptide sequences. The collision-induced dissociation (CID) spectra of peptides are usually assigned with the help of various bioinformatics tools that implement sequencing algorithms and peptide fragmentation models. The existing sequencing programs are based on rather limited fragmentation models that only offer a poor approximation of the rich dissociation chemistry of peptides.[2] It is now widely accepted[3] in the peptide-sequencing community that these limitations often lead to erroneous assignments of peptides and proteins when the current sequencing algorithms are used. The resulting uncertainty in the evaluation of the raw MS/MS data is one of the major limiting factors in large-scale protein identification studies. Advancing gas-phase peptide chemistry into maturity would no doubt change this situation by offering detailed fragmentation mechanisms and characteristics that could put MS/MS-based peptide sequencing onto a much more robust basis.

The current understanding of gas-phase peptide chemistry has recently been summarized in the *pathways in competition*

[†] German Cancer Research Center.
[‡] Wichita State University.
[§] University of Kansas.
[||] University of Toronto.

(1) (a) Aebersold, R.; Goodlett, D. R. *Chem. Rev.* **2001**, *101*, 269. (b) Hunt, D. F.; Yates, J. R., 3rd; Shabanovitz, J.; Winston, S.; Hauer, C. R. *Proc. Natl. Acad. Sci. U.S.A.* **1986**, *83*, 6233.
(2) Paizs, B.; Suhai, S. *Mass Spectrom. Rev.* **2005**, *24*, 508.
(3) (a) Steen, H.; Mann, M. *Nat. Rev. Mol. Cell. Biol.* **2004**, *5*, 699. (b) Nesvizhskii, A. E.; Vitek, O.; Aebersold, R. *Nat. Methods* **2007**, *4*, 787.

 10.1021/ja805074d CCC: $40.75

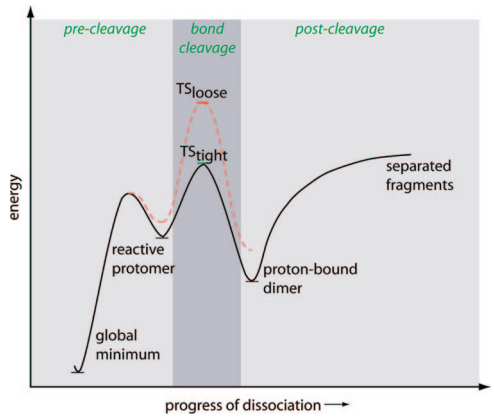

Figure 1. Various phases of peptide ion dissociation as considered by the "pathways in competition" fragmentation model (PIC).[2]

fragmentation model (PIC).[2] PIC provides a general framework for understanding gas-phase peptide chemistry, taking into account specific features of individual peptide fragmentation pathways (PFPs) and their interaction. PIC considers the dissociation of peptides to be a complicated process. This complexity can be more easily understood with PIC when viewed as having three well-defined phases: (1) the pre-cleavage phase, (2) the (amide) bond-cleavage phase, and (3) the post-cleavage phase (Figure 1).

The energetically most favored peptide ion structures rarely undergo direct fragmentation.[2] Instead, in the pre-cleavage phase of peptide dissociation, proton-transfer reactions and other structural transitions populate those species that fragment directly. The related proton-transfer pathways are the main tenet of the *mobile proton* fragmentation model.[4] In this sense, the mobile proton model should be considered as a predecessor of PIC. Upon excitation, the ionizing proton is transferred from an unreactive site of higher gas-phase basicity (an Arg, Lys, or His side chain or the N-terminal amino group) to form energetically less favored but reactive backbone-amide-protonated species. Fast proton transfer to various backbone amide bonds usually results in MS/MS spectra rich in sequence informative *b*, *y*, and *a* ions.[5] However, sequestration of the added proton(s) by basic amino acid side chains often leads to information-poor MS/MS spectra. These substantially different fragmentation characteristics can be explained by considering the mobility of added protons. On the other hand, prediction of fragment ion abundances requires detailed consideration of the bond-cleavage and post-cleavage phases of peptide fragmentation as well and thus a much deeper understanding of the related chemistry.

The bond-cleavage phase (e.g., the mechanism, energetics, and kinetics of amide bond cleavage) has recently been studied in detail.[2,6,7] The dissociation pathways that are active under the usual low-collision-energy conditions commonly lead to formation of N-terminal fragments that are terminated with five- or six-membered rings. These rearrangement-type reactions usually proceed via "*tight*" transition structures (TS_{tight} in Figure 1). These have lower critical energies but are entropically less favored than direct bond cleavage-type reactions involving "*loose*" TSs (TS_{loose} in Figure 1). The critical energy of the latter is usually higher than that of the former, but entropic factors can make the two reaction channels competitive if the peptide precursors are excited well above the threshold energies of the lowest-energy fragmentation channels. Typical examples of "tight" and "loose" TSs are those associated with the b_n-y_m[7b] and a_n-y_m[7a] amide bond cleavage pathways, respectively.

The post-cleavage phase of peptide fragmentation has received surprisingly limited attention in the past, despite the rich chemistry involved. Under low-energy collision conditions, the fragments created by amide bond cleavage are expected to form proton-bound dimers (PBDs). These PBDs can also undergo various reactions. Most importantly, the fate of the added proton(s) is decided by the dissociation kinetics of the PBDs and can be assessed [2,7c,8] if the gas-phase basicities (GB) or proton affinities (PA) of the fragments are available. On a qualitative basis, the fragment with the higher GB will remain protonated with higher probability than the fragment with the lower GB. However, the fragments kept together in PBDs can also undergo various reactions, including association reactions and H/D exchange.[9] New fragments can be created by further dissociation of the primary fragments, leading to secondary products such as internal fragments,[10] amino acid specific immonium ions,[11] and smaller members of the *b*, *a*, and *y* series.

Furthermore, primary linear fragments can rearrange by forming macrocyclic isomers that can in turn open up at various bonds and create a range of distinct linear forms. This phenomenon was first described by Boyd and co-workers in their landmark papers[12] on peptides containing lysine and ornithine residues. By investigating the CID characteristics of substance P, peaks that are uninterpretable in terms of the known sequence were observed. MS/MS/MS experiments and acetylation of the free amino groups were used to demonstrate that the side chain of the lysine residue of substance P plays an important role in formation of the above peaks. A mechanism

(4) (a) Dongré, A. R.; Jones, J. L.; Somogyi, Á.; Wysocki, V. H. *J. Am. Chem. Soc.* **1996**, *118*, 8365. (b) Wysocki, V. H.; Tsaprailis, G.; Smith, L. L.; Breci, L. A. *J. Mass Spectrom.* **2000**, *35*, 1399. (c) Burlet, O.; Yang, C. Y.; Gaskell, S. J. *J. Am. Soc. Mass Spectrom.* **1992**, *3*, 337. (d) Tang, X.; Boyd, R. K. *Rapid Commun. Mass Spectrom.* **1992**, *6*, 651. (e) Johnson, R. S.; Krylov, D.; Walsh, K. A. *J. Mass Spectrom.* **1995**, *30*, 386. (f) Harrison, A. G.; Yalcin, T. *Int. J. Mass Spectrom.* **1997**, *165*, 339. (g) Csonka, I. P.; Paizs, B.; Lendvay, G.; Suhai, S. *Rapid Commun. Mass Spectrom.* **2000**, *14*, 417. (h) Jorgensen, T. J. D.; Gardsvoll, H.; Ploug, M.; Roepstorff, P. *J. Am. Chem. Soc.* **2005**, *127*, 2785.

(5) (a) Roepstorff, P.; Fohlmann, J. *J. Biomed. Mass Spectrom.* **1984**, *11*, 601. (b) Biemann, K. *Biomed. Environ. Mass Spectrom.* **1988**, *16*, 99.

(6) (a) Yalcin, T.; Khouw, C.; Csizmadia, I. G.; Peterson, M. R.; Harrison, A. G. *J. Am. Soc. Mass Spectrom.* **1995**, *6*, 1165. (b) Yalcin, T.; Csizmadia, I. G.; Peterson, M. R.; Harrison, A. G. *J. Am. Soc. Mass Spectrom.* **1996**, *7*, 233. (c) Nold, M. J.; Wesdemiotis, C.; Yalcin, T.; Harrison, A. G. *Int. J. Mass Spectrom. Ion Processes* **1997**, *164*, 137. (d) Vaisar, T.; Urban, J. *J. Mass Spectrom.* **1998**, *33*, 505. (e) Farrugia, J.; O'Hair, R. A. J.; Reid, G. *Int. J. Mass Spectrom.* **2001**, *210−211*, 71.

(7) (a) Paizs, B.; Suhai, S. *Rapid Commun. Mass Spectrom.* **2001**, *15*, 651. (b) Paizs, B.; Suhai, S. *Rapid Commun. Mass Spectrom.* **2002**, *16*, 375. (c) Paizs, B.; Suhai, S. *Rapid Commun. Mass Spectrom.* **2002**, *16*, 1699. (d) Paizs, B.; Suhai, S. *J. Am. Soc. Mass Spectrom.* **2004**, *15*, 103.

(8) Harrison, A. G. *J. Mass Spectrom.* **1999**, *34*, 577.

(9) (a) Cooper, T.; Talaty, E.; Grove, J.; Suhai, S.; Paizs, B.; Van Stipdonk, M. *J. Am. Soc. Mass Spectrom.* **2006**, *17*, 1654. (b) Bythell, B. J.; Barofsky, D. F.; Pingitore, F.; Wang, P.; Wesdemiotis, C.; Paizs, B. *J. Am. Soc. Mass Spectrom.* **2007**, *18*, 1291.

(10) Ballard, K. D.; Gaskell, S. J. *Int. J. Mass Spectrom. Ion Processes* **1991**, *111*, 173.

(11) Ambihapathy, K.; Yalcin, T.; Leung, H.-W.; Harrison, A. G. *J. Mass Spectrom.* **1997**, *32*, 209.

(12) (a) Tang, X.-J.; Thibault, P.; Boyd, R. K. *Anal. Chem.* **1993**, *65*, 2824. (b) Tang, X.-J.; Boyd, R. K. *Rapid Commun. Mass Spectrom.* **1994**, *8*, 678.

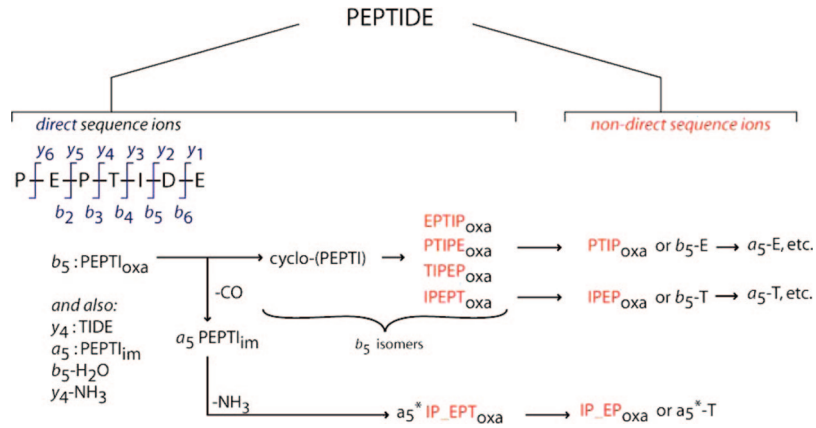

Figure 2. Graphical representation of the nomenclature[15] that distinguishes *direct sequence* and *nondirect sequence* ions generated by CID of protonated peptides. The hypothetical peptide "PEPTIDE" is used to present typical examples of direct and nondirect fragments. The single-letter amino acid code is used to represent peptide and fragment ion sequences.

involving nucleophilic attack of the Lys side chain amine group on the presumed $-CO^+$ moiety of *b* ions to form a macrocyclic *b* isomer followed by ring opening at other amide bonds to create rearranged *b* ions was proposed.[12] These scrambled isomers can then fragment further to form peaks that are uninterpretable in terms of the known sequence assuming "typical" fragmentation. Vázquez and co-workers[13] showed that formation of cyclic *b* isomers can be initiated by the N-terminal amino group as well. Glish and co-workers[14] discovered that not only *b* but also *a* ions can rearrange by elimination of ammonia on the $a \rightarrow a^*$ pathway. For example, CID of protonated Leu-enkephalin (YGGFL) under some circumstances results in the $a_4 - NH_3 - G$ fragment at *m*/*z* 323 that is formed from the a_4 ion by loss of ammonia and one of the internal G residues. A mechanism was proposed that involves S_N2-type nucleophilic attack by the C-terminal imine group on the α-carbon of the N-terminal Y residue, forming a cyclic $a_4 - NH_3$ isomer via loss of NH_3, and subsequent opening of the ring to allow loss of the former internal G residue.[14]

In a recent communication to this journal,[15] we showed that *b* ions with C-terminal oxazolone rings can cyclize to form cyclic peptide isomers. CID of protonated YAGFL-NH_2 resulted in fragment ions that cannot be directly derived from the primary peptide structure. Instead, they could be explained by assuming cyclization of the b_5 ion and subsequent ring opening. The breakdown graphs of protonated *cyclo*-(YAGFL) and b_5 of YAGFL-NH_2 were found to be very similar, suggesting that cyclic *b* isomers play an important role in peptide fragmentation. Modeling suggested that the cyclization of the linear *b* isomer proceeds through a TS with relatively low critical energy.

Recently, Polfer et al.[16] studied the structure of b_4 and a_4 fragments of Leu-enkephalin by infrared multiphoton dissociation (IRMPD) spectroscopy and modeling. It was shown that both fragments form macrocyclic isomers. The cyclic a_4 isomer is formed by nucleophilic attack of the N-terminal amino group on the carbon center of the protonated imine group. Along with the backbone amide bonds, this species contains a secondary amine group, and the backbone macrocycle can in principle open up at various bonds, giving rise to the formation of scrambled linear a_4 isomers. Enjalbal and co-workers[17] have recently studied the fragmentation characteristics of a large number of peptides in a quadrupole time-of-flight mass spectrometer. These authors found that numerous peptides fragment on pathways that involve cyclic peptide *b* ion isomers. Recent ion mobility spectrometry (IMS) studies[18] provided further structural details on N-terminal peptide fragments. Gaskell and co-workers[18a] have shown that the arrival time distributions of protonated *cyclo*-(YAGFL) and b_5 of YAGFL-NH_2 are very similar, lending strong support to the *b*-ion cyclization mechanism. IMS experiments on the a_4 ion of YAGFL-NH_2 indicated the presence of at least two structurally different ion populations. In similar experiments, Polfer et al.[18b] investigated the a_4 fragment of YGGFL and found three structurally different ion populations that include the linear and cyclic isomers. However, a third structure present in the IMS spectrum could not be assigned on the basis of the available data.

To facilitate discussion of the related chemistry, a new nomenclature[15] (worked out in Figure 2 for a hypothetical peptide PEPTIDE) was proposed to distinguish between *direct sequence* and *nondirect sequence* ions of protonated peptides. The mass-to-charge ratios and structures of direct sequence ions can be derived directly from the known structure of the parent peptide. Members of the *b* (e.g., b_5 or $PEPTI_{oxa}$), *y* (e.g., y_4 or TIDE), and *a* (e.g., a_5 or $PEPTI_{im}$) ion series are considered to be direct sequence ions (the subscripts "oxa" and "im" denote fragments with oxazolone and imine C-termini, respectively). Satellites of the *b* and *y* ion series, such as internal fragments (e.g., PTI_{oxa}) and immonium ions (e.g., I_D, the imine of aspartic acid) or their fragments derived by loss of small neutrals (mostly H_2O and NH_3, e.g., $b_5 - H_2O$ or $y_4 - NH_3$), are considered to be direct sequence ions as well. On the other hand, the structures and mass-to-charge ratios of nondirect sequence ions cannot be derived directly from the known primary peptide sequence. These fragments are formed from rearranged primary fragments via further dissociation. The nondirect sequence ions discovered

(13) Yagüe, J.; Paradela, A.; Ramos, M.; Ogueta, S.; Marina, A.; Barahona, F.; López de Castro, J. A.; Vázquez, J. *Anal. Chem.* **2003**, *75*, 1524.
(14) Vachet, R. W.; Bishop, B. M.; Erickson, B. W.; Glish, G. L. *J. Am. Chem. Soc.* **1997**, *119*, 5481.
(15) Harrison, A. G.; Young, A. B.; Bleiholder, B.; Suhai, S.; Paizs, B. *J. Am. Chem. Soc.* **2006**, *128*, 10364.
(16) Polfer, N. C.; Oomens, J.; Suhai, S.; Paizs, B. *J. Am. Chem. Soc.* **2007**, *129*, 5887.
(17) (a) Mouls, L.; Subra, G.; Aubagnac, J.-L.; Martinez, J.; Enjalbal, C. *J. Mass Spectrom.* **2006**, *41*, 1470. (b) Mouls, L.; Aubagnac, J.-L.; Martinez, J.; Enjalbal, C. *J. Proteome Res.* **2007**, *6*, 1378.
(18) (a) Riba-Garcia, I.; Giles, K.; Bateman, R. H.; Gaskell, S. J. *J. Am. Soc. Mass Spectrom.* **2008**, *19*, 609. (b) Polfer, N. C.; Bohrer, B. C.; Plasencia, M. D.; Paizs, B.; Clemmer, D. E. *J. Phys. Chem. A* **2008**, *112*, 1286.

so far include scrambled fragments of the *b* type (e.g., $IPEP_{oxa}$) and *a** type [e.g., IP_EP_{oxa}, where the shorthand notation XY_ indicates that the former C-terminal imine of an *a* ion is transferred to the N-terminus during the rearrangement and a new N-terminus is formed (more details provided below)]. This nomenclature is used throughout this report to identify rearrangements of *b* and *a* ions.

Recent peptide identification software interprets nondirect sequence ions as members of the direct *b*, *a*, or *y* series, and the related chemistry is not implemented in the fragmentation models used for sequencing. Therefore, nondirect sequence ions in peptide MS/MS spectra can lead to erroneous peptide sequencing, thereby contributing to the significant false-positive rate of high-throughput protein identification studies in proteomics.[19] The known sequence-scrambling fragmentation pathways produce nondirect sequence ions that originate from N-terminal primary fragments. Recently, Olsen and Mann[20a] have applied MS/MS/MS experiments in a linear ion trap to increase the confidence of peptide identification by fragmenting the primary dissociation products. They found that C-terminal primary fragments (mainly *y* ions) produce useful additional information but N-terminal fragments generate MS/MS/MS spectra that are rarely understandable by considering typical fragmentation. This practical finding can be attributed to the occurrence of nondirect sequence ions. It is envisaged that the sequence information obtained from MS/MS/MS spectra will be more widely used for peptide and protein identification in the future, especially in large-scale phosphoproteome studies[20b] and top-down identification of intact proteins.[20c,d]

In this paper, we expand our previous study[15] to investigate the important details of *b*- and *a*-type scrambling pathways. A combined experimental and modeling approach has been used to study the formation and opening of the related cyclic isomers and how the scrambling pathways interact with the typical fragmentation channels. First, CID of protonated FAGFL-NH_2 with and without an ^{15}N label on the N-terminal amino group was examined to unambiguously identify the amine eliminated initially to generate the b_5 product. A series of permuted "sequence isomers" of YAGFL was then synthesized and examined to compare the *m/z* values of product ions generated by dissociation of the b_5 ions. The relative intensities of the product ions were compared in order to determine the sensitivity of these spectra to the initial peptide sequence. The same series of peptides was used to investigate potential rearrangement(s) of a_5 ions. Modeling was then used to determine the relative energies of the respective reactive protomers, transition states, and post-dissociation products to rationalize the trends observed in the CID experiments.

Experimental and Computational Section

Experimental work was performed at the Department of Chemistry, Wichita State University (Wichita, KS), the Department of Chemisty, University of Kansas (Lawrence, KS), and the University of Toronto (Toronto, Canada). Electrospray ionization mass spectrometry (ESI-MS) and CID experiments were conducted on a quadrupole ion trap (IT) and two different quadrupole time-of-flight (QqTOF) instruments. The molecular dynamics simulations and quantum-chemical calculations were carried out at the German Cancer Research Center (Heidelberg, Germany). Both the experimental and theoretical strategies are briefly described below.

Peptide Synthesis and Preparation. Peptides with sequences FAGFL-NH_2, YAGFL-NH_2, AGLFY-NH_2, GFLYA-NH_2, FLYAG-NH_2, LYAGF-NH_2, and N-terminally ^{15}N-labeled FAGFL-NH_2 (^{15}N-FAGFL-NH_2) were synthesized by conventional solid-phase methods using either Rink amide- or Fmoc-G-loaded solid-phase resins (purchased from Sigma Chemical, St. Louis, MO, and used as received), Fmoc-protected amino acids, and a custom-built, multiple-reaction-vessel peptide synthesis apparatus. Peptides, once cleaved from the resin, were used without subsequent purification in the CID studies. The sequences of peptides synthesized in-house were verified using the multiple-stage CID of $[M + Ag]^+$, which is an effective approach for sequencing from the C-terminus in the gas phase.[21] YAGFL-NH_2 was also obtained from Bachem Biosciences (King of Prussia, PA), and *cyclo*-(YAGFL) was obtained from Celtek Peptides (Nashville, TN).

For the quadrupole ion trap CID experiments, solutions of each peptide were prepared by dissolving the appropriate amount of solid material in a 1:1 (v/v) mixture of HPLC-grade MeOH (Aldrich Chemical, St. Louis, MO) and deionized H_2O to produce final concentrations of 10^{-5} to 10^{-4} M. Peptide solutions were infused into the ESI-MS instrument at a flow rate of 5 μL/min using the incorporated syringe pump. For QqTOF experiments, peptides were dissolved in 1:1 CH_3OH/0.1% aqueous formic acid and introduced into the electrospray source at flow rates of 25 and 80 μL min^{-1} for the qTOF-2 and QSTAR instruments, respectively.

Mass Spectrometry and Collision-Induced Dissociation. The IT multiple-stage CID experiments were conducted on a Finnigan LCQ-Deca mass spectrometer (ThemoFinnigan, San Jose, CA). The atmospheric pressure ionization stack settings for the LCQ (lens voltages, quadrupole and octapole voltage offsets, etc.) were optimized for maximum $[M + H]^+$ transmission to the ion trap mass analyzer by using the autotune routine within the LCQ Tune program. Following the instrument tuning, the spray needle voltage was maintained at +5 kV, the N_2 sheath gas flow at 25 units (arbitrary for the Finnigan systems, corresponding to ~0.375 L/min), and the capillary (desolvation) temperature at 200 °C. Helium was used as the bath/buffer gas to improve trapping efficiency and as the collision gas for CID experiments.

The CID studies (MS/MS and MS^n) were performed as follows: The $[M + H]^+$ ions were isolated for the initial CID stage (MS/MS) using an isolation width of *m/z* 0.9−1.2. Product ions selected for subsequent CID (MS^n experiments) were isolated using widths of *m/z* 1.0−1.3. The exact width was chosen empirically and reflected the best compromise between high $(M + H)^+$ abundance and the isolation of a single isotopic peak. The (mass) normalized collision energy, which defines the amplitude of the RF energy applied to the end-cap electrodes in the CID experiment, was set between 20 and 25%, which roughly corresponds to 0.80−0.99 V with the instrument calibration used in this study. The activation Q (as labeled by ThermoFinnigan, used to adjust the q_z value for the precursor ion) was set at 0.30. Subsequent CID stages were performed using similar activation parameter settings. The activation time employed at each CID stage was 30 ms.

MS^2 and MS^3 experiments also were carried out on QSTAR (MDS Sciex, Concord, Canada) and qTOF-2 (Waters Corp., Milford, MA) mass spectrometers, both of which feature a QqTOF configuration. On both QqTOF platforms, MS^3 experiments were performed by using interface/cone region CID to produce fragment ions from $[M + H]^+$ followed by mass selection of the b_5 ion using

(19) (a) Taylor, G. K.; Goodlett, D. R. *Rapid Commun. Mass Spectrom.* **2005**, *19*, 3420. (b) Publication Guidelines for the Analysis and Documentation of Peptide and Protein Identifications. http://www.mcponline.org/misc/ParisReport_Final.shtml (accessed Dec 3, 2008).

(20) (a) Olsen, J. V.; Mann, M. *Proc. Natl. Acad. Sci. U.S.A.* **2004**, *101*, 13417. (b) Ulintz, P. J.; Bodenmiller, B.; Andrews, P. C.; Aebersold, R.; Nesvizhskii, A. I. *Mol. Cell Proteomics* **2008**, *7*, 71. (c) Macek, B.; Waanders, L. F.; Olsen, J. V.; Mann, M. *Mol. Cell Proteomics* **2006**, *5*, 949. (d) Han, X. M.; Jin, M.; Breuker, K.; McLafferty, F. W. *Science* **2006**, *314*, 109.

(21) Barr, J. M.; Van Stipdonk, M. J. *Rapid Commun. Mass Spectrom.* **2002**, *16*, 566.

Scheme 1. Fragmentation Pathways of Protonated YAGFL-NH_2[a]

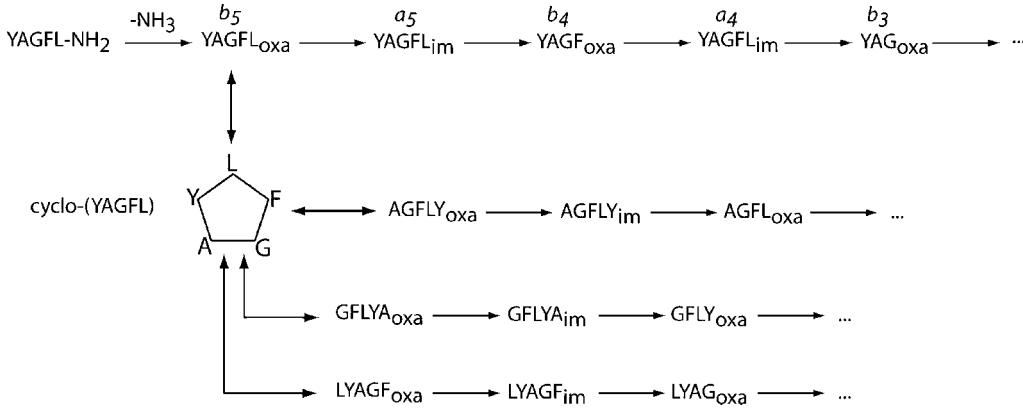

[a] Loss of ammonia leads to the $YAGFL_{oxa}$ b_5 ion, which can further dissociate on the $b_5 \rightarrow a_5 \rightarrow b_4 \rightarrow a_4 \rightarrow b_3 \rightarrow$... reaction cascade (direct sequence ions). Alternatively, $YAGFL_{oxa}$ can cyclize to form protonated *cyclo*-(YAGFL), which can open up at positions other than the L−Y amide bond to form scrambled linear oxazolones such as $AGFLY_{oxa}$ or $GFLYA_{oxa}$. Further fragmentation of these ions leads to nondirect sequence ions.

the first quadrupole mass analyzer (Q) for subsequent collisional activation of the species in the quadrupole collision cell (q). The product ions generated by fragmentation of b_5 within the quadrupole collision cell were then analyzed by the time-of-flight mass analyzer.

On the qTOF-2 platform, the b_5 ions generated from protonated peptapeptide amides were subjected to CID at 15 and 25 eV collision energy (laboratory frame). Precursor ions were selected for cone/source fragmentation using an *m/z* window of 4 units, and the cone voltage used for source-region CID was chosen empirically to optimize production of sufficient b_5 ion intensity for subsequent CID in the collision-cell region. Once optimized, the same cone fragmentation voltage was used for the entire group of peptides. Ar was used in the collision cell at a pressure sufficient to attentuate the ion signal to 20%.

CID experiments on the QSTAR platform were performed in a similar fashion, but the voltage applied in the collision cell was varied to produce breakdown graphs for mass-selected fragment ions. In the QSTAR experiments, nitrogen was used as the nebulizing gas and the drying gas as well as the collision gas in the quadrupole collision cell.

Computational Details. A recently developed conformational search engine[2,7,9] devised to deal with protonated peptides was used to scan the potential energy surfaces (PESs) of protonated *cyclo*-(YAGFL) and its fragments. These calculations started with molecular dynamics simulations on the above ions using the Insight II program (Biosym Technologies, San Diego, CA) in conjunction with the AMBER force field,[22] modified in-house in order to enable the study of structures with oxygen- and nitrogen-protonated amide bonds, imine and oxazolone groups, and amide bond cleavage TSs. During the dynamics calculations, we used simulated annealing techniques to produce candidate structures for further refinement, applying full geometry optimization using the AMBER force field. These optimized structures were analyzed by a conformer family search program developed by us. This program groups optimized structures into families within which the most important characteristic torsion angles of the molecule are similar. The most stable species in the families were then fully optimized at the PM3, HF/3-21G, B3LYP/6-31G(d), and B3LYP/6-31+G(d,p) levels, and the conformer families were regenerated at each level. The total energies of the lowest-energy structures are presented in Tables S1 and S2 in the Supporting Information. It should be noted that the Gaussian suite of programs[23] was used for all of the ab initio and DFT calculations.

For the energetically most preferred structures, we performed frequency calculations at the B3LYP/6-31G(d) level of theory. The relative energies were calculated by correcting the B3LYP/6-31+G(d,p) total energies for zero-point vibrational energy (ZPE) and/or thermal and entropy contributions determined from the unscaled B3LYP/6-31G(d) frequencies.

Results and Discussion

In our previous communication,[15] we presented experimental and computational data on the dissociation chemistry of protonated YAGFL-NH_2 (Scheme 1). Upon excitation, this peptide ion fragments nearly exclusively by loss of ammonia. The resulting $YAGFL_{oxa}$ b_5 ion eliminates CO to form $YAGFL_{im}$ (a_5), which dissociates further to form smaller *b* and *a* ions such as $YAGF_{oxa}$ (b_4), $YAGF_{im}$ (a_4), YAG_{oxa} (b_3,), and so on. In a competing reaction channel, nucleophilic attack of the N-terminal amino group on the charged C-terminal oxazolone group leads to cyclization of $YAGFL_{oxa}$. The resulting *cyclo*-(YAGFL) isomer (Scheme 1) can reopen at amide bonds other than the newly formed amide bond between the L and Y residues. This leads to b_5 isomers such as $AGFLY_{oxa}$, $GFLYA_{oxa}$, $FLYAG_{oxa}$, and $LYAGF_{oxa}$, in which the original primary sequence has been scrambled. Further degradation of such scrambled b_5 structures leads to formation of nondirect sequence ions (Scheme 1) such as $AGFL_{oxa}$ or $LYAG_{oxa}$. The fragmentation behavior[15] of protonated YAGFL-NH_2 could satisfactorily be explained in terms of the reaction pattern shown in Scheme 1. Here we provide further experimental data that support the *b* ion cyclization−reopening mechanism.

1. CID of Linear Peptides and Fragments. (a) Labeling Experiments on FAGFL-NH_2. To determine whether the loss of NH_3 from a protonated peptide amide like YAGFL-NH_2 to form the b_5 fragment (Scheme 1) involves elimination of the N- or C-terminal $-NH_2$ moiety, CID of FAGFL-NH_2 and ^{15}N-FAGFL-NH_2 (i.e., without and with a ^{15}N label on the N-terminal amino group) was examined. Figure 3 shows the spectra generated in the IT mass spectrometer (MS^2 stage). The dominant product ions appear at *m/z* 536 and 537 for FAGFL-NH_2 and ^{15}N-FAGFL-NH_2, respectively, corresponding to loss of 17 u ($^{14}NH_3$) from $[M + H]^+$. Also observed were peaks at *m/z* 423 and 424 for FAGFL-NH_2 and ^{15}N-FAGFL-NH_2, respectively, which reflect elimination of the C-terminal Leu residue (130 u) to produce b_4. The dominant loss of 17 u from both the unlabeled and labeled versions of the peptide demonstrates that the reaction pathway does not involve the N-terminal amino group but instead occurs through loss of NH_3 at the C-terminus of the peptide.

(22) Case, D. A.; et al. *AMBER 99*; University of California: San Francisco, 1999.
(23) Frisch, M. J.; et al. *Gaussian 03*; Gaussian, Inc.: Pittsburgh, PA, 2003.

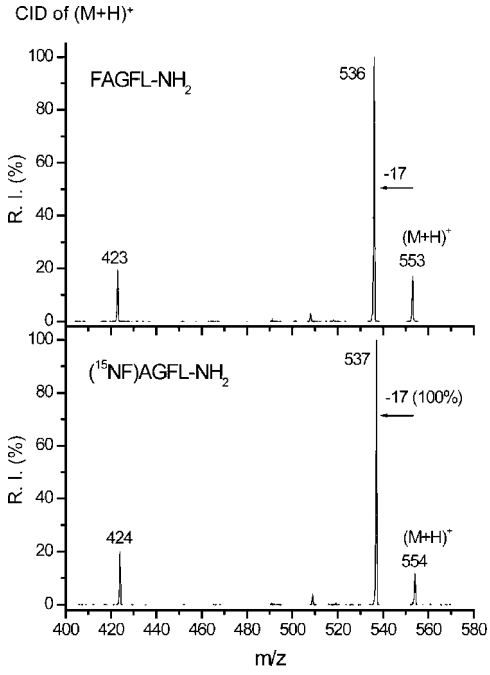

Figure 3. CID of protonated FAGFL-NH_2 and ^{15}N-FAGFL-NH_2 in an IT instrument.

(b) CID of the b_5 Fragments of Sequence Isomers of YAGFL-NH_2. To further test our hypothesis concerning the cyclization pathway of *b* ions and to evaluate the influence of the peptide sequence on the formation of nondirect sequence ions, permuted isomers of YAGFL-NH_2, including AGFLY-NH_2, GFLYA-NH_2, FLYAG-NH_2, and LYAGF-NH_2, were synthesized and investigated in MS^2 and MS^3 experiments. CID of the singly charged forms of these peptides leads to the production of more or less abundant b_5 ions, for which fragmentation patterns were generated in MS^3 experiments in the IT instrument or in pseudo-MS^3 experiments in the QqTOF instruments. Figure 4 shows the IT CID spectra (MS^3 stage) for the b_5 ions derived from the five sequence isomers. The product ion distributions for the five peptides are remarkably similar. The a_5 and a_5* species (*m*/*z* 524 and 507, respectively), which are fragments characteristic of the decomposition of b_n ions, were generated from each version of b_5. More interesting was the appearance of product ions at *m*/*z* 389, 439, and 481, which correspond to loss of 163 u (residue mass of Y), 113 u (residue mass of L) and 71 u (residue mass of A), respectively. These species were observed at similar relative abundances regardless of the sequence of amino acids in the precursor peptide. The loss of the Y residue (to form the product ion at *m*/*z* 389) is apparently favored despite the fact that the residue occupies different sequence positions (including three in the interior) within the investigated peptides.

This observation is most easily rationalized with the hypothesis that the b_5 species rapidly adopts the cyclic structure after formation from $[M + H]^+$. To test this idea, a comparison with the MS/MS spectrum of protonated *cyclo*-(YAGFL) obtained under similar experimental conditions (the last panel of Figure 4) was made. The product ion distribution of *cyclo*-(YAGFL) is remarkably similar to those obtained for the b_5 ions of YAGFL-NH_2 and its permuted isomers. This strongly suggests that the linear b_5 species rapidly converts to the cyclic form, which fragments further upon excitation.

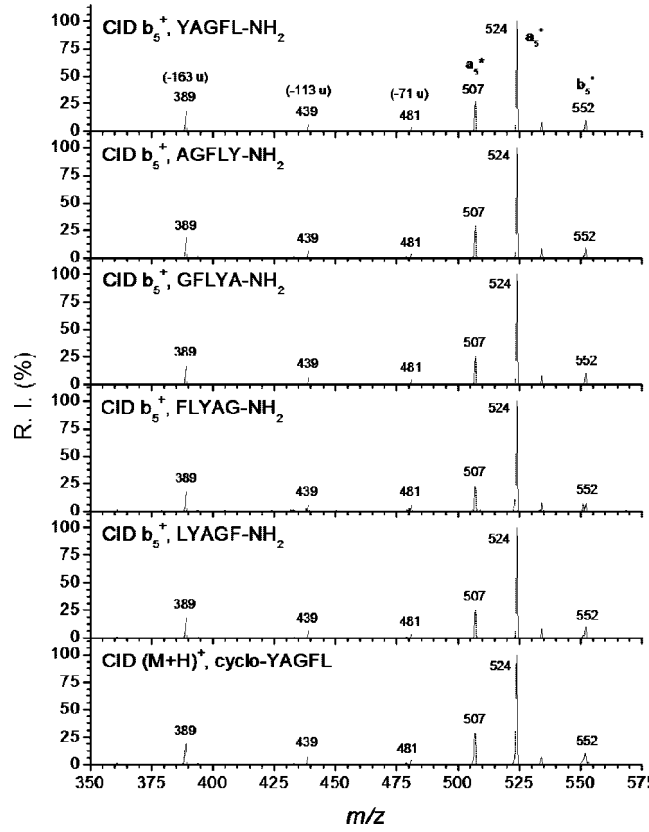

Figure 4. CID of b_5 ions derived from sequence isomers of YAGFL-NH_2. The sequence of each precursor peptide is shown with its respective spectrum. The last panel displays the MS/MS spectrum of protonated *cyclo*-(YAGFL) for comparison. CID was performed using the IT instrument. No ion signals were observed below *m*/*z* 350.

The fragmentation behavior of the same b_5 ions was also investigated using the QqTOF-type instrument. Figure S1 in the Supporting Information shows the spectra of b_5 ions generated from $[M + H]^+$ by cone/source fragmentation and then selected for CID in the collision cell of the QqTOF instrument. As for the experiments conducted on the IT instrument, the fragmentation patterns generated from the b_5 ions in the QqTOF instrument under relatively low energy CID conditions (15 eV applied, laboratory frame) were remarkably similar. The QqTOF spectra display the conventional a_5 and a_5* species and fragments at *m*/*z* 389, 439, and 481 (corresponding to the elimination of Y, L, and A, respectively). Also observed in the QqTOF spectrum was a peak at *m*/*z* 405, consistent with activation of a pathway involving elimination of F (loss of 147 u) that was not observed in the IT experiments. Again, CID of protonated *cyclo*-(YAGFL) gives a fragment ion distribution that is very similar to those obtained for the b_5 ions of YAGFL-NH_2 and its sequence isomers. The salient observation is that under low-energy conditions in the IT or QqTOF instruments, the CID spectra generated from the group of sequence isomers are virtually identical, in terms of both the product ions generated and their relative intensities (for a given instrument).

This behavior can have a disastrous effect on peptide sequencing using the limited fragmentation models currently implemented in database search software. For example, typical fragmentation of the b_5 ion of FLYAG-NH_2 (formally FLY-AG_{oxa}) is expected to result in direct sequence ions such as b_4 (*m*/*z* 495.3), a_4 (*m*/*z* 467.3), b_3 (*m*/*z* 424.2), and b_2 (*m*/*z* 261.2).

Current database search software attempts to identify the FLYAG sequence motif by looking for matches between these theoretical *m/z* values and those observed experimentally. As shown in Figure 4 and Figure S1 in the Supporting Information, none of the above theoretical *m/z* values could be matched to peaks in the IT and QqTOF (15 eV collision energy) CID spectra of the b_5 ion of FLYAG-NH_2. Figure S2 in the Supporting Information shows the CID spectrum of the same b_5 ion obtained at 18 eV collision energy. This spectrum contains much more abundant peaks than the one recorded at 15 eV collision energy, but the direct sequence ions of FLYAG-NH_2 are nearly completely missing (only the peak at *m/z* 261 with minimal abundance can be assigned as a direct sequence b_2 ion). Evidently, fragmentation models that do not consider the *b*-type scrambling pathways will falsely assign such dissociation patterns.

Cyclization of the $FLYAG_{oxa}$ structure seems to be complete for the IT and QqTOF instruments under low-energy conditions. Furthermore, it is likely that reopening of the cyclic peptide b_5 isomer is not favored at the G−F amide bond, which is formed during cyclization of this ion. This actually leads to complete loss of the original sequence information upon CID. The spectra in Figure 4 and Figure S1 in the Supporting Information suggest that the linear oxazolone isomers rapidly cyclize and that the corresponding MS/MS/MS fragmentation pattern is determined by the reactivity of the cyclic form. The fragments produced by the cyclic form can only be explained by considering a multitude of linear fragmenting structures. In general, this suggests that extreme care should be exercised when evaluating sequencing information obtained from MS^3 experiments. While such information can be straightforward to interpret for *y* ions (truncated peptides), this is far from the case if the automated peak selection algorithm of the mass spectrometer picks up *b* ions for further fragmentation.

2. Structure and Fragmentation Pathways of Protonated *cyclo*-(YAGFL). The experimental data presented in the previous sections and the recent literature[15−18] strongly suggest that *b* ions can undergo cyclization to form cyclic peptide isomers. The fragmentation chemistry of cyclic peptides[24] is of interest on its own because these compounds can have significant biological activity. This could be monitored by MS/MS in a straightforward manner if the related dissociation mechanisms were fully understood. To explore the related chemistry in detail, the structure and reactivity of protonated *cyclo*-(YAGFL) have been investigated using our combined experimental and theoretical approach.

(a) CID of Protonated *cyclo*-(YAGFL). The major fragmentation product of protonated *cyclo*-(YAGFL) (Figures 4 and 5 and Figure S1 in the Supporting Information) is the $[MH - CO]^+$ ion at low collision energies. Loss of CO is followed by two major and a few minor dissociation cascades. The most abundant cascade involves formation of the fragments $[MH - Y]^+$, $[MH - Y - CO]^+$, and $[MH - Y - L]^+$, which can be associated with ring opening at the Y−A amide bond [−CH($CH_2C_6H_5OH$)−CO−NH−CHMe−] to form the linear $AGFLY_{oxa}$ isomer and its fragmentation products ($AGFL_{oxa}$, $AGFL_{im}$, and AGF_{oxa}, respectively). Less abundant but still significant is the reaction cascade involving the fragments $[MH - L]^+$, $[MH - L - CO]^+$, $[MH - L - CO - NH_3]^+$, and $[MH - L - F]^+$. This channel is associated with ring opening at the L−Y amide bond to form the linear $YAGFL_{oxa}$ isomer, which further fragments to form $YAGF_{oxa}$, $YAGF_{im}$, $YAGF_{im}-NH_3$, and YAG_{oxa}. The CID spectra in Figures 4 and 5 and Figure S1 in the Supporting Information suggest that the dissociation channels involving the linear $GFLYA_{oxa}$ and $LYAGF_{oxa}$ isomers are much less active and that fragmentation through $FLYAG_{oxa}$ is negligible. CID of protonated *cyclo*-(YAGFL) at higher collision energies results in a large number of fragments. For most of the smaller fragments, a few independent assignments are possible, making spectrum assignment difficult.

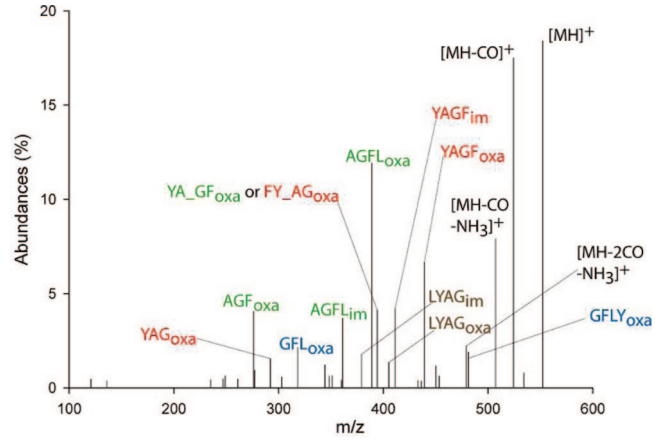

Figure 5. CID of protonated *cyclo*-(YAGFL) at 22 eV collision energy (laboratory scale) in a QqTOF instrument. The fragment assignments are color coded: fragments derived from the $YAGFL_{oxa}$, $AGFLY_{oxa}$, $GFLYA_{oxa}$, and $LYAGF_{oxa}$ oxazolone forms are shown in red, green, blue, and brown, respectively.

It is worth noting here that CID of protonated *cyclo*-(YAGFL) produces abundant $[MH - CO]^+$, $[MH - CO - NH_3]^+$, and $[MH - 2CO - NH_3]^+$ ions, even at higher collision energies. It is very likely that these ion populations are made up of various isomers, such as $AGFLY_{im}$, $YAGFL_{im}$, $LYAGF_{im}$, and $GFLYA_{im}$ for $[MH - CO]^+$. We cannot distinguish among these isomers with our current tools and therefore have no information on the composition of these ion populations. This should be considered when discussing the activity of degradation pathways of protonated *cyclo*-(YAGFL) via the possible open oxazolone forms.

(b) Potential Energy Surface of Protonated *cyclo*-(YAGFL). The PES of protonated *cyclo*-(YAGFL) was scanned, and the relative energies (E_{rel}) of its amide oxygen and nitrogen protonation sites and ring-opening transition structures were calculated (Figure 6 and Table S1 in the Supporting Information). These calculations assumed that all of the amide bonds of *cyclo*-(YAGFL) are in the trans isomerization state. The global minimum on the PES of protonated *cyclo*-(YAGFL) is one of the L−Y amide oxygen-protonated species (Figure S3 in the Supporting Information). Protonation at the F−L, G−F, and Y−A amide oxygens requires a similar energy (~1 kcal mol^{-1}), while species protonated at the A−G amide oxygen are energetically less favored. Protonation at the amide nitrogens is possible at internal energies spanning the range 12.1−17.7 kcal mol^{-1}.

Upon excitation, these amide nitrogen-protonated species become populated, and the corresponding carbonyl carbon can

(24) (a) Eckart, K. *Mass Spectrom. Rev.* **1994**, *13*, 23. (b) Ngoka, L. C. M.; Gross, M. L. *J. Am. Soc. Mass Spectrom.* **1999**, *10*, 732. (c) Williams, S. M.; Brodbelt, J. S. *J. Am. Soc. Mass Spectrom.* **2004**, *15*, 1039. (d) Jegorov, A.; Paizs, B.; Žabka, M.; Kuzma, M.; Giannakopulos, A. E.; Derrick, P. J.; Havlíček, V. *Eur. J. Mass Spectrom* **2003**, *9*, 105. (e) Jegorov, A.; Paizs, B.; Kuzma, M.; Žabka, M.; Landa, Z.; Šulc, M.; Havlíček, V. *J. Mass Spectrom* **2004**, *39*, 949.

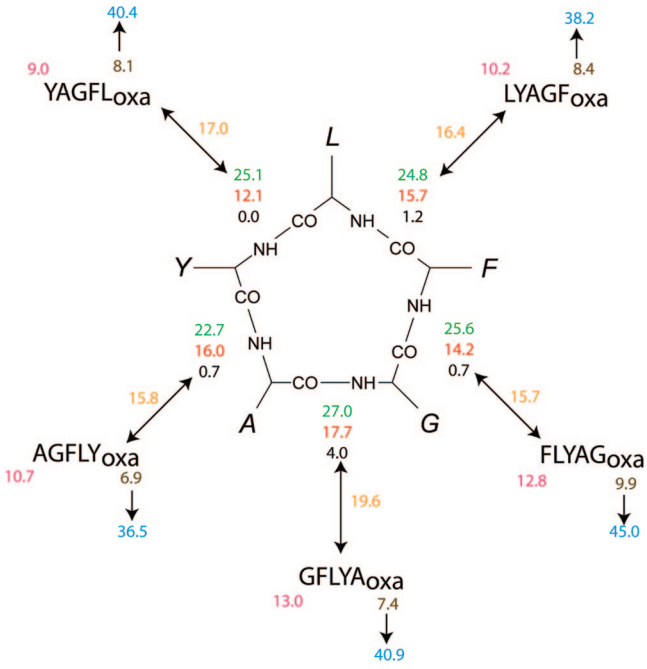

Figure 6. Relative energies (kcal mol^{-1}) of various species on the PES of protonated *cyclo*-(YAGFL). The *cyclo*-peptide backbone is shown explicitly, while amino acid side chains are denoted by *Y*, *A*, *G*, *F*, and *L*, respectively. Relative energies of the amide oxygen and nitrogen protonation sites of *cyclo*-(YAGFL) are given in black and red, respectively. Relative energies of the TSs of the ring-opening reactions are given in green. These reactions lead to the linear b_5 isomers YAGFL$_{oxa}$, AGFLY$_{oxa}$, GFLYA$_{oxa}$, FLYAG$_{oxa}$, and LYAGF$_{oxa}$, for which relative energies are presented for the N-terminal amino (purple) and C-terminal oxazolone (brown) protonation sites as well as for the corresponding $b_5 \rightarrow a_5$ TSs (blue). The cyclization barriers of the linear isomers (given in orange) can be calculated as the differences between the relative energies of the appropriate ring-opening TSs and the corresponding linear isomers.

be attacked by the adjacent amide oxygen. This induces cleavage of the protonated amide bond and leads to formation of an oxazolone ring on a b_n-y_m-type ring-opening pathway (Scheme 2).[2] The energetically most favored ring-opening TS (E_{rel} = 22.7 kcal mol^{-1}, Figure S4 in the Supporting Information) leads to the AGFLY$_{oxa}$ linear isomer (Scheme 2), while structures LYAGF$_{oxa}$, YAGFL$_{oxa}$, FLYAG$_{oxa}$, and GFLYA$_{oxa}$ can be formed via TSs at E_{rel} = 24.8, 25.1, 25.6, and 27.0 kcal mol^{-1}, respectively. It is worth noting here that only small energy differences are predicted for these ring-opening TSs.

In the next step, the energies of the N-terminal amino and C-terminal oxazolone protonation sites of possible linear *b* isomers (YAGFL$_{oxa}$, AGFLY$_{oxa}$, GFLYA$_{oxa}$, FLYAG$_{oxa}$, and LYAGF$_{oxa}$) and their CO-loss TSs were determined. These linear forms are energetically less favored than the cyclic isomers protonated at the amide oxygen atoms. The energetically most favored linear isomer is AGFLY$_{oxa}$ with C-terminal oxazolone protonation (E_{rel} = 6.9 kcal mol^{-1}, Figure 6). This computational result is in agreement with the ion mobility data obtained by Riba-Garcia et al.,[18a] which showed similar arrival time distributions for protonated *cyclo*-(YAGFL) and the b_5 ion of YAGFL-NH$_2$. This suggests that the cyclic form of the b_5 ion of YAGFL-NH$_2$ is stable on the millisecond time scale of the ion mobility instrument.

As the energies given in Figure 6 suggest, the YAGFL$_{oxa}$, AGFLY$_{oxa}$, GFLYA$_{oxa}$, FLYAG$_{oxa}$, and LYAGF$_{oxa}$ linear forms have to overcome cyclization barriers of 17.0, 15.8, 19.6, 15.7, and 16.4 kcal mol^{-1}, respectively, to form the macrocyclic isomer. This clearly explains the rapid cyclization observed for the linear b_5 isomers, since the cyclic isomer is energetically more favored than any of the open forms and the associated cyclization barriers are lower than those observed for the usual bond-breaking reactions.

For each linear isomer, protonation at the C-terminal oxazolone site is energetically favored over protonation at the N-terminal amino group. The most stable linear isomers span a relatively narrow internal energy range of 7−10 kcal mol^{-1}. The critical energies of the CO-loss reactions[2,7] are 36.5, 38.2, 40.4, 40.9, and 45.0 kcal mol^{-1} for AGFLY$_{oxa}$, LYAGF$_{oxa}$, YAGFL$_{oxa}$, GFLYA$_{oxa}$, and FLYAG$_{oxa}$, respectively. It should be noted that the critical energies for CO loss span a wider range than those of the ring-opening reactions.

(c) Comparison of Our Experimental and Computational Data on Protonated *cyclo*-(YAGFL). Figure 6 presents critical data related to the stability and reactivity of protonated *cyclo*-(YAGFL) and the corresponding linear oxazolone-terminated forms. It should be noted that opening of the macrocycle and loss of CO from the linear isomers are the first two steps on the dissociation pathways leading to degradation products. The macro-ring of protonated *cyclo*-(YAGFL) can open up along b_n-y_m-type pathways after proton transfer to amide nitrogens, as shown in Scheme 2. The linear isomers can further fragment by loss of CO to form species that are terminated by an imine group at the C-terminus (e.g., YAGFL$_{im}$). These species can then further fragment by loss of ammonia or to the next lower oxazolone. Our CID data on protonated *cyclo*-(YAGFL) (Figures 4 and 5 and Figure S1 in the Supporting Information) suggest that the energetically and kinetically most favored ring-opening pathway leads to formation of AGFLY$_{oxa}$, which fragments further to form the [MH − Y]$^+$, [MH − Y − CO]$^+$, and [MH − Y − L]$^+$ ions. This phenomenon is nicely explained by our computational data, which indicate that the ring opening at the Y−A amide bond involves the lowest-energy TS (22.7 kcal mol^{-1}, Figure 6) among the five possibilities. Furthermore, AGFLY$_{oxa}$ features the lowest-energy TS for CO loss (36.5 kcal mol^{-1}, Figure 6) among the five linear forms.

As described above, fragments belonging to the FLYAG$_{oxa}$ linear form are nearly completely missing from the spectrum of protonated *cyclo*-(YAGFL). Furthermore, CID of b_5 of FLYAG-NH$_2$ results in a spectrum that contains hardly any direct sequence ions. These observations can easily be rationalized in terms of the high barrier (35.1 kcal mol^{-1}, Figure 6), which is calculated as the difference between the energies of the CO-loss TS (E_{rel} = 45.0 kcal mol^{-1}) and the oxazolone-protonated form of FLYAG$_{oxa}$ (E_{rel} = 9.9 kcal mol^{-1}), which is associated with CO loss from the FLYAG$_{oxa}$ isomer. It is very likely that this species preferentially undergoes cyclization to *cyclo*-(YAGFL) (for which the barrier is 15.7 kcal mol^{-1}) rather than degradation.

Our CID data further indicate that ring opening at the L−Y amide bond is more favored than at other amide bonds such as F−L, A−G, and G−F. Our computational data, however, indicate that cleavage at the L−Y and F−L amide bonds should occur to a similar extent, since the calculated ring-opening TS energies (25.1 and 24.8 kcal mol^{-1}) and linear oxazolone energies (8.1 and 8.4 kcal mol^{-1}) are very close to one another. This apparent contradiction can be resolved by studying the fate of the [MH − CO]$^+$ ion populations, as described below.

3. Structures and Scrambling Pathways of a_n and a_n* Ions. In principle, not only *b* but also *a* and *a** fragments can undergo various cyclization and rearrangement reactions. This

Scheme 2. Opening of the Macro-Ring of Protonated *cyclo*-(YAGFL) at the Y−A and L−Y Amide Bonds, Subsequent CO Loss from the $AGFLY_{oxa}$ and $YAGFL_{oxa}$ Linear Isomers, and Formation of $AGFL_{oxa}$ ($[MH - Y]^+$) and $YAGF_{oxa}$ ($[MH - L]^+$), Respectively[a]

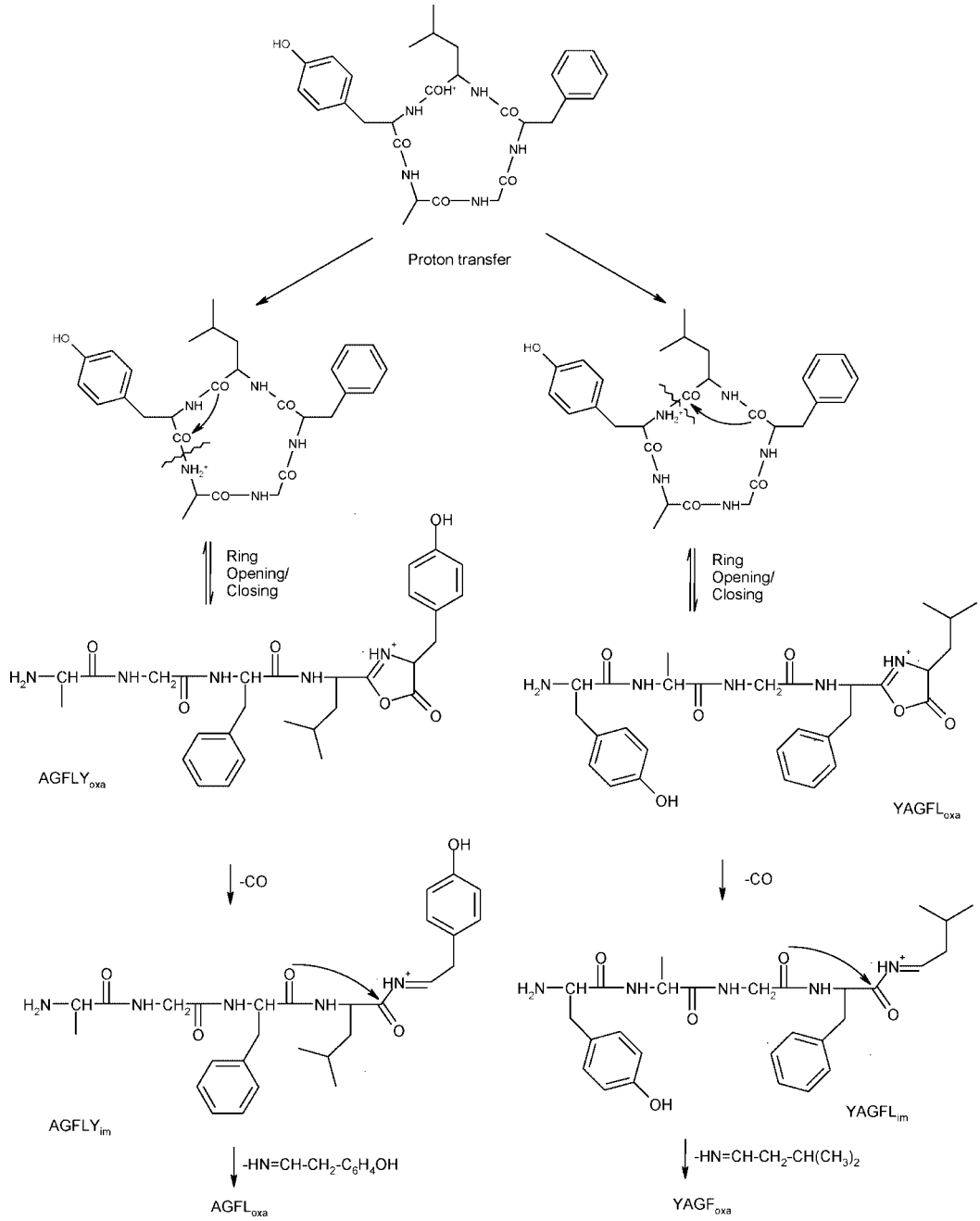

[a] Similar reaction cascades can be generated for the $GFLYA_{oxa}$, $FLYAG_{oxa}$, and $LYAGF_{oxa}$ cases.

phenomenon was first observed by Glish and co-workers,[14] who found that CID of YGGFL can lead to the $a_4 - NH_3 - G$ fragment. Recently, Polfer et al.[16] investigated the structure of a_4 of YGGFL using IRMPD spectroscopy and modeling techniques. The IRMPD spectrum of a_4 could only be explained if one assumes that the a_4 population contains both linear and cyclic isomers. Very recent IMS studies[18] indicate that *a* ions feature multiple structures.

In the following, we will investigate the structure and reactivity of the $[MH - CO]^+$ fragments of protonated *cyclo*-(YAGFL) and the a_5 ions of YAGFL-NH_2 and its permutated isomers. Under low-energy collision conditions, the majority of *a* fragments are formed from *b* ions by loss of CO.[11,25] This means that *a* ion populations are usually affected by scrambling activities of their parent *b* ions. For *cyclo*-(YAGFL), this means that the macro-ring opens up at various amide bonds to form linear oxazolone species ($YAGFL_{oxa}$, $AGFLY_{oxa}$, $GFLYA_{oxa}$, and $LYAGF_{oxa}$) that further fragment by loss of CO (to form $YAGFL_{im}$, $AGFLY_{im}$, $GFLYA_{im}$, and $LYAGF_{im}$). In other words, a discussion of the structure and reactivity of *a* ions must always consider the possibility that the parent *b* population has already undergone *b*-type scrambling.

(25) Vachet, R. W.; Ray, K. L.; Glish, G. L. *J. Am. Soc. Mass Spectrom.* **1998**, *9*, 341.

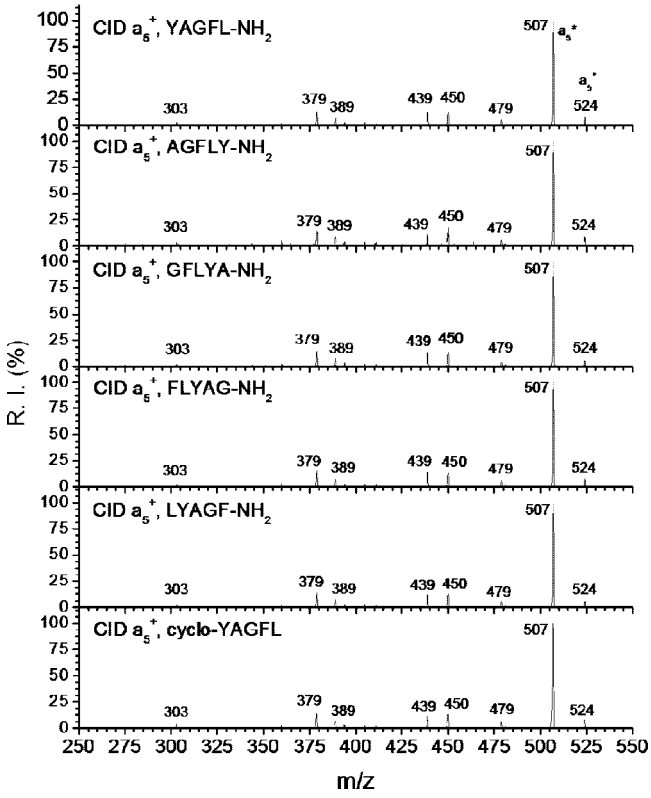

Figure 7. CID of a_5 ions derived from sequence isomers of YAGFL-NH_2. The sequence of each precursor peptide is shown with its respective spectrum. The last panel displays the MS/MS spectrum of $[MH - CO]^+$ of *cyclo*-(YAGFL) for comparison. CID was performed using the IT instrument.

(a) CID of the a_5 Fragments of the Sequence Isomers of YAGFL-NH_2. CID of the b_5 ions of the permuted isomers of YAGFL-NH_2 produces nearly identical fragment ion distributions, as shown in Figure 4 and Figure S1 in the Supporting Information. Not fully unexpectedly, CID of the corresponding a_5 ions in the IT instrument follows the same trend of producing fragment ion patterns for the five peptide isomers that are indistinguishable (Figure 7). This effect is most likely due to the rapid cyclization of the linear b_5 ions to form the macrocyclic isomer, which reopens to give the resulting linear isomer population that further fragments to form a_5 ions. This speculation is supported by the results for CID of the $[MH - CO]^+$ ion of *cyclo*-(YAGFL) shown in the last panel in Figure 7. The fragment ion distribution of the $[MH - CO]^+$ ion of *cyclo*-(YAGFL) is not distinguishable from those observed for the a_5 ions of the permuted isomers of YAGFL-NH_2.

Typical fragmentation of linear a_5 ions results in direct sequence ions on the a_5 (a_5*) → b_4 → a_4 (a_4*) → b_3 cascade. Our studies described above suggest that only the $YAGFL_{oxa}$, $AGFLY_{oxa}$, $GFLYA_{oxa}$, and $LYAGF_{oxa}$ b_5 isomers are formed and can therefore undergo loss of CO to form the corresponding imines ($YAGFL_{im}$, $AGFLY_{im}$, $GFLYA_{im}$, and $LYAGF_{im}$, respectively). For each of these sequence isomers, a distinct a_5 (a_5*) → b_4 → a_4 (a_4*) → b_3 cascade can be generated, leading to a large number of possible fragments. However, only two of these are indeed observed in Figure 7: $AGFL_{oxa}$ (*m/z* 389) and $YAGF_{oxa}$ (*m/z* 439) that are formed from $AGFLY_{im}$ and $YAGFL_{im}$ by loss of the C-terminal Y and L imines, respectively. The other fragment ions in Figure 7 can be assigned as a_5* − *CO* (*m/z* 479), a_5* − *G* (*m/z* 450), a_5* − *G* − *A* (*m/z* 379), and a_5* − *F* − *G* (*m/z* 303). Data for QqTOF CID of the

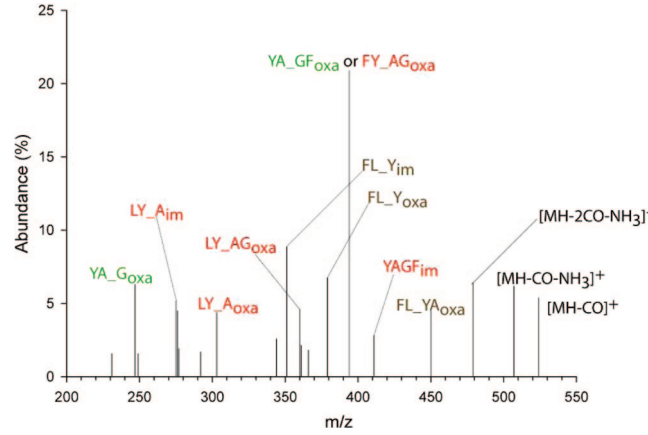

Figure 8. CID mass spectrum (25 eV laboratory-frame collision energy) of the $[MH - CO]^+$ ion of protonated *cyclo*-(YAGFL). The fragment assignments are color coded: fragments derived from the $YAGFL_{oxa}$, $AGFLY_{oxa}$, $GFLYA_{oxa}$, and $LYAGF_{oxa}$ oxazolone forms are shown in red, green, blue, and brown, respectively.

a_5 ions generated from the permuted isomers of YAGFL-NH_2 are shown in Figure S5 in the Supporting Information. Again, these spectra are very similar to one another. Additional fragments compared with the IT spectra appear at *m/z* 394, 360, and 344 and can be assigned as a_5* − *L*, a_5* − *F*, and a_5* − *Y*, respectively.

Figure 8 displays CID data for the $[MH - CO]^+$ ion of *cyclo*-(YAGFL) recorded at higher collision energy (25 eV, laboratory frame). Because of the larger excitation energy, more pronounced fragmentation is observed. As in the case of the fragmentation of the $[MH]^+$ ion (Figure 5), fragments formed from the linear $AGFLY_{oxa}$ and $YAGFL_{oxa}$ isomers are abundant. A new feature of the spectrum in Figure 8 is that many fragments that can be derived from $LYAGF_{oxa}$ appear. This suggests that the $[MH - CO]^+$ ion population consists of a substantial fraction of $LYAGF_{im}$.

The fragmentation pathways of the a_5 ion of YAGFL-NH_2 and its permuted isomers and of the $[MH - CO]^+$ ion of *cyclo*-(YAGFL) are summarized in Scheme 3. The fragments in Figures 7 and 8 and Figure S5 in the Supporting Information can be almost entirely assigned by considering *b*-type scrambling of the appropriate parent population and subsequent $a_n \rightarrow a_n$*-type rearrangements. The isolated a_5 ions primarily fragment along ammonia-loss pathways that lead to a rearranged linear structure in which the former C-terminal residue is relocated to the N-terminus.[14] Such a_n* ions feature the CHR═N−CHR′− moiety (denoted by XY_ in Figure 1 and Scheme 3) at their N-terminus and an oxazolone group at the C-terminus. The CHR═N−CHR′− moiety is likely to be more stable than the C-terminal oxazolone group, and therefore, dissociation of a_n* ions is likely to be dominated by gradual degradation of their C-termini. The related fragmentation pathways (Scheme 3) offer a reasonable explanation for the majority of the fragments in Figures 7 and 8 and Figure S5 in the Supporting Information. In other words, no *a*-type scrambling is required to explain the fragmentation patterns of the a_5 ions of YAGFL-NH_2 and its sequence isomers. In the following, we will attempt to understand the underlying chemistry with the help of modeling techniques and to characterize the related fragmentation pathways and their interaction.

(b) Potential Energy Surfaces of $YAGFL_{im}$, $LYAGF_{im}$, and $AGFLY_{im}$. In order to gain a deeper understanding of the chemistry of the linear and cyclic a_5 ions, the PESs of $YAGFL_{im}$,

Scheme 3. Fragmentation Pathways of the a_5 Fragments of YAGFL-NH_2 and Its Permuted Isomers and of the $[MH - CO]^+$ Ion of *cyclo*-(YAGFL)[a]

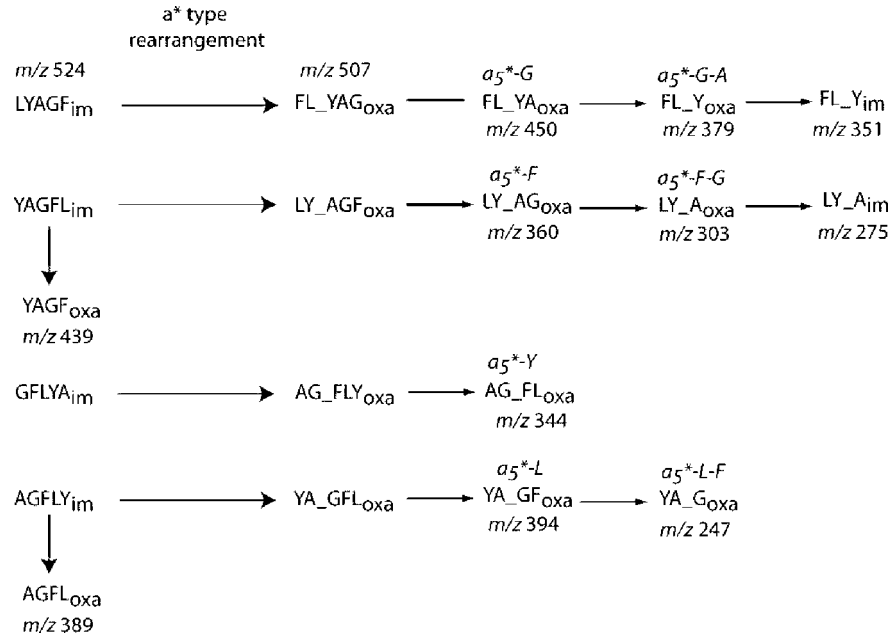

[a] As a result of *b*-type scrambling of their parent ions, these fragments form a mixture of $YAGFL_{im}$, $AGFLY_{im}$, $GFLYA_{im}$, and $LYAGF_{im}$. Only a small fraction of these linear imines fragment on direct pathways to form the next lower oxazolone-terminated ions ($AGFL_{oxa}$ and $YAGF_{oxa}$). Rather, $a_n \rightarrow a_n$*-type rearrangements form linear isomers terminated by the CHR═N−CHR′− and oxazolone moieties at the N- and C-termini. These species further fragment at their C-termini along pathways specific to the oxazolone group.

$LYAGF_{im}$, and $AGFLY_{im}$ were characterized in detail (Figure 9 and Table S2 in the Supporting Information). It is to be noted here that the relative energies in Figure 9 are given with respect to the energetically most favored cyclic a_5 ion of a given sequence and are not given relative to a common structure. This is due to the fact that once formed, the $YAGFL_{im}$, $LYAGF_{im}$, and $AGFLY_{im}$ structures cannot interconvert from one to another, so their chemistries should be represented by different PESs.

Upon formation from their parent oxazolones, $YAGFL_{im}$, $LYAGF_{im}$, and $AGFLY_{im}$ feature protonated C-terminal imine groups that play a critical role in the reactivity of *a* ions. These structures can undergo proton-transfer reactions to populate the species protonated at the N-terminal amino group (shown for $YAGFL_{im}$ in Scheme 4). Alternatively, the adjacent N-terminal amide oxygen can attack the C-terminal carbonyl to cleave the $-OC-NH^+-$ bond (shown for $YAGFL_{im}$ in Scheme 4) to form the next lower *b* ion. The last possibility involves nucleophilic attack of the N-terminal amino group on the carbon center of the protonated imine (shown for $YAGFL_{im}$ in Scheme 5). This reaction leads to the cyclic $YAGFL_{im}$, $LYAGF_{im}$, and $AGFLY_{im}$ isomers.

For all of the investigated imines, the energetically most favored structure is the cyclic isomer (Figure 9 and Table S2 in the Supporting Information). The relative energies of the linear forms vary significantly with the actual sequence. For $YAGFL_{im}$, the relative energy of the most favored linear structure is 1.4 kcal mol^{-1}, while for $LYAGF_{im}$ and $AGFLY_{im}$, the cyclic form is 6−8 kcal mol^{-1} more stable than any of the linear structures. The backbone of the cyclic isomers contains four amide bonds and a secondary amine group (Figure 9). The macro-ring can in principle open up at any of these bonds after proton transfer. It should be noted that ring opening at the secondary amine group recovers the original linear structure and therefore does not lead to scrambling of the primary sequence. Ring opening at the amide bonds, on the other hand, would lead to major rearrangement and formation of scrambled structures, as shown in Scheme 5 for the F−L amide bond of the cyclic isomer of $YAGFL_{im}$.

The ring-opening reactions of the cyclic structure were explored in detail for $YAGFL_{im}$. The energetically most favored ring-opening TS is at the secondary amine group (E_{rel} = 14.5 kcal mol^{-1}, reaction I in Scheme 5). Cleavage at the amide bonds requires formation of N-protonated species and occurs on b_n-y_m-type pathways. This reaction was studied for the F−L amide bond. The energetically most favored F−L amide N-protonated species is at 15.4 kcal mol^{-1}, which is above the critical energy of 14.5 kcal mol^{-1} for ring opening at the secondary amine group (Scheme 5, reaction I). Furthermore, the relative energy of the corresponding b_n-y_m-type ring-opening TS is 32.8 kcal mol^{-1}. It is likely that the magnitude of the critical energies of the b_n-y_m-type ring-opening TSs are similar for the A−G and G−F amide bonds. This means that ring opening at amide bonds is not competitive with ring opening at the secondary amine group of the cyclic a_5 ion.

From the point of view of sequence scrambling, this suggests that the a_n-type scrambling PFP in Scheme 5 is not active. It is very likely that a significant fraction of the a_5 ion population is in the cyclic form in mass spectrometers. However, these species tend to open up at the secondary amine group upon excitation and recover their original linear structure, which then fragments further. These mechanistic considerations fully support our fragment assignments in Figures 7 and 8 and Figure S5 in the Supporting Information, which were based on *b*-type scrambling and $a_n \rightarrow a_n$*-type rearrangement pathways without considering *a*-type scrambling.

The stabilities of the $YAGFL_{im}$, $LYAGF_{im}$, and $AGFLY_{im}$ structures are also determined by the relative energies of the TSs on their lowest-energy degradation pathways. To investigate this effect, we explored the $a_5 \rightarrow b_4$-type pathways for

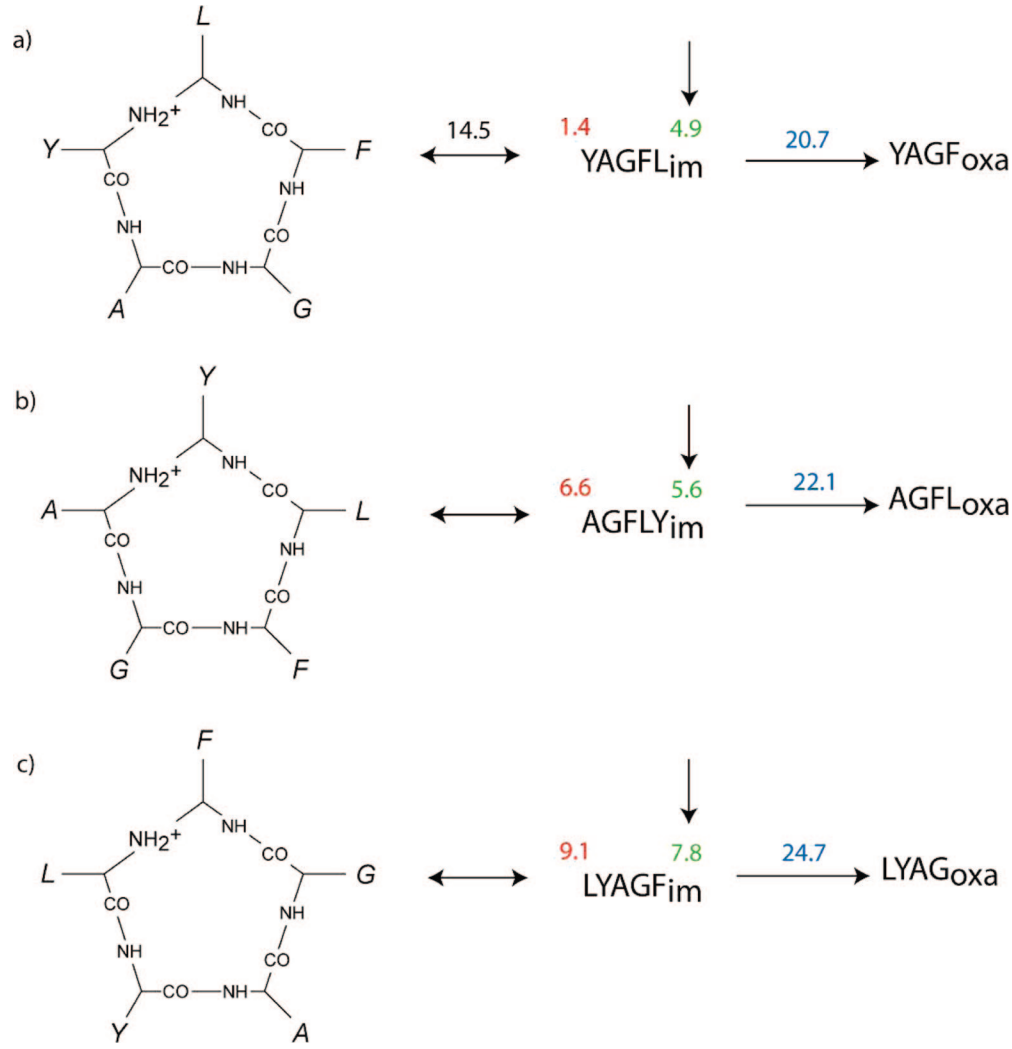

Figure 9. Relative energies (kcal mol^{-1}) of various species on the PESs of (a) YAGFL$_{im}$, (b) LYAGF$_{im}$, and (c) AGFLY$_{im}$. The cyclic backbone is shown explicitly, while amino acid side chains are denoted by *Y*, *A*, *G*, *F*, and *L*, respectively. For each species, the cyclic form is the energetically most favored structure and represents the zero of energy. Relative energies of the linear C-terminal imine- and N-terminal amino-protonated structures are given in red and green, respectively. Relative energies of the TSs for the C-terminal imine-loss reactions are given in blue.

YAGFL$_{im}$, LYAGF$_{im}$, and AGFLY$_{im}$, and the corresponding TS energies are also displayed in Figure 9. Nucleophilic attack of the adjacent N-terminal amide oxygen on the C-terminal carbonyl CO (Scheme 4, shown for YAGFL$_{im}$) leads to the formation of a new oxazolone ring (YAGF$_{oxa}$ in Scheme 4) and loss of the C-terminal imine. The relative energies of the $a_5 \rightarrow b_4$-type TSs are 20.7, 22.1, and 24.7 kcal mol^{-1} for YAGFL$_{im}$, AGFLY$_{im}$, and LYAGF$_{im}$, respectively. These data suggest that LYAGF$_{im}$ is kinetically more stable than the other two isomers and is likely to significantly contribute to the overall a_5 population. In section 2(c) it was shown that fragments associated with LYAGF$_{oxa}$ are less abundant in the CID of protonated *cyclo*-(YAGFL) or the b_5 ions of YAGFL-NH$_2$ than expected on the basis of our computational results. This apparent contradiction is now resolved by considering the increased stability of LYAGF$_{im}$ with respect to YAGFL$_{im}$ and AGFLY$_{im}$. Of course, even the more stable LYAGF$_{im}$ isomer can be fragmented if appropriate excitation energy is applied, as is seen in the CID of the [MH $-$ CO]$^+$ ion of protonated *cyclo*-(YAGFL) (Figure 8).

(c) $a_n \rightarrow a_n$*-Type Rearrangement Pathways: The Vachet−Glish Mechanism.[14] In the following, we briefly discuss the mechanism and energetics of the $a_n \rightarrow a_n$*-type rearrangement pathways. Glish and co-workers[14] have studied CID of a number of peptides (primarily Leu-enkephalin analogues) and found that nondirect sequence fragments that could be derived from a_n and a_n* ions were formed. The mechanism proposed by these authors is depicted in Scheme 6 for YAGFL$_{im}$, with some modifications introduced by us to replace the unstable −CO−NH−CHR−CO$^+$ moieties with oxazolone rings. Nucleophilic attack of the C-terminal imine N on the N-terminal α-carbon in an S$_N$2-type reaction leads to loss of ammonia and formation of a macrocyclic product. The corresponding transition structure (Figure S6a in the Supporting Information) involves inversion of the corresponding chiral center at a relative energy of 51.2 kcal mol^{-1}. Despite the many attempts made, no lower-energy TS of this type was found. We note here that the $a_5 \rightarrow b_4$-type TS for YAGFL$_{im}$ (Scheme 4) is at $E_{rel} = 20.7$ kcal mol^{-1}, and thus, the S$_N$2-type ammonia loss at $E_{rel} = 51.2$ kcal mol^{-1} is very unlikely to compete with this process. The S$_N$2 ammonia-loss TS results in a cyclic species that has a fixed-charge immonium nitrogen. The adjacent carbonyl C is a likely target of nucleophilic attack by the G−F carbonyl O. This b_n−y_m-like reaction opens up the macro-ring and leads to the open isomer (LY_AGF$_{oxa}$) shown in Scheme 6.

Scheme 4. Formation of $YAGF_{oxa}$ from $YAGFL_{im}$[a]

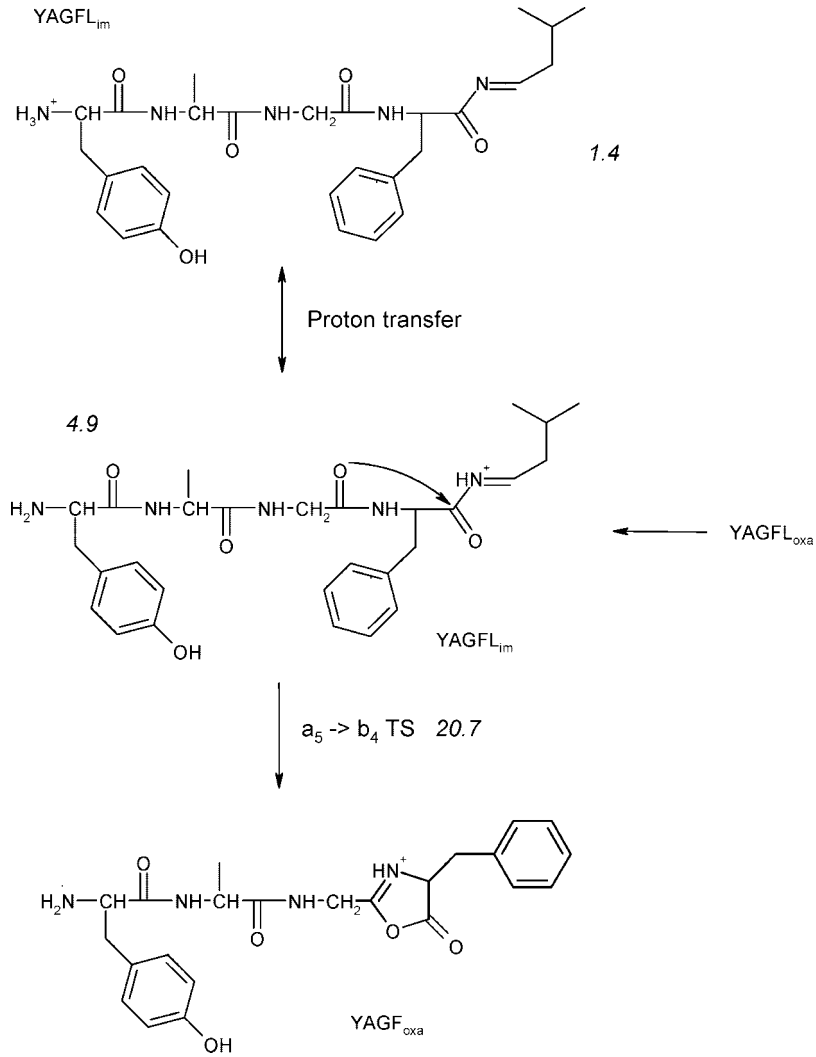

[a] Relative energies (kcal mol^{-1}) are given in italics for the amino- and imine-protonated forms and the $a_5 \rightarrow b_4$-type TS.

(d) $a_n \rightarrow a_n$*-Type Rearrangement Pathways: The PBD Mechanism.[9] The formation of the a_3* ion of protonated GGGG has recently been studied[9] by a combined experimental and modeling strategy, and a new $a_n \rightarrow a_n$* mechanism was proposed that is shown in Scheme 7 for linear $YAGFL_{im}$. On the product wing of the $a_5 \rightarrow b_4$-type TS (for more details see above), one finds proton-bound dimers of $YAGF_{oxa}$ and the imine of L. Under low-energy conditions, these PBDs can rearrange to form species where the N-terminal amino group of the neutral oxazolone and the carbon center of the protonated L imine are close to each other. One of the energetically most favored such structures is shown in Figure S6b in the Supporting Information. The charged imine group is effectively solvated by the N-terminal amino and carbonyl groups of the $YAGF_{oxa}$ oxazolone, which actually folds around the much smaller imine. This geometrical arrangement brings the N-terminal amino group of the oxazolone close (3.320 Å) to the carbon of the charged imine. This surprisingly stable PBD is at a relative energy of 5.2 kcal mol^{-1} with respect to the cyclic isomer of $YAGFL_{im}$.

Nucleophilic attack of the amino N on the imine carbon leads to reassociation of the oxazolone and imine to form a new a_5 isomer that bears an oxazolone group at its C-terminus. It is noteworthy that the corresponding TS (Figure S6c in the Supporting Information) has a relative energy of 18.2 kcal mol^{-1} and is energetically much more favored than the S_N2-type Vachet−Glish ammonia-loss TS (51.2 kcal mol^{-1}) discussed above. After the reassociation step, a rapid proton transfer to the N-terminal amino group (E_{rel} = 9.0 kcal mol^{-1}, Figure S6d in the Supporting Information) and subsequent loss of ammonia result in LY_AGF_{oxa}. The corresponding ammonia-loss TS (Figure S6e in the Supporting Information) is at E_{rel} = 19.3 kcal mol^{-1}.

Conclusions

(1) Our labeling experiments on FAGLF-NH_2 indicate that loss of ammonia from the parent ion involves the C-terminal NH_2 moiety. This reaction leads to linear *b* ions (such as $FAGLF_{oxa}$ or $YAGLF_{oxa}$) with a five-member oxazolone ring at the C-terminus.

(2) CID of the b_5 ions derived from the peptides YAGFL-NH_2, AGFLY-NH_2, GFLYA-NH_2, FLYAG-NH_2, and LYAGF-NH_2 and of protonated *cyclo*-(YAGFL) leads to the same spectrum in the IT instrument, even though these ions are formally different. The same behavior is observed in QqTOF instruments if low excitation energies are used. This phenomenon strongly suggests that rapid cyclization of the primary linear oxazolones takes place to form the cyclic peptide isomer of the corresponding b_5 ions. Cyclization of

Scheme 5. Formation of the Cyclic Isomer of $YAGFL_{im}$[a]

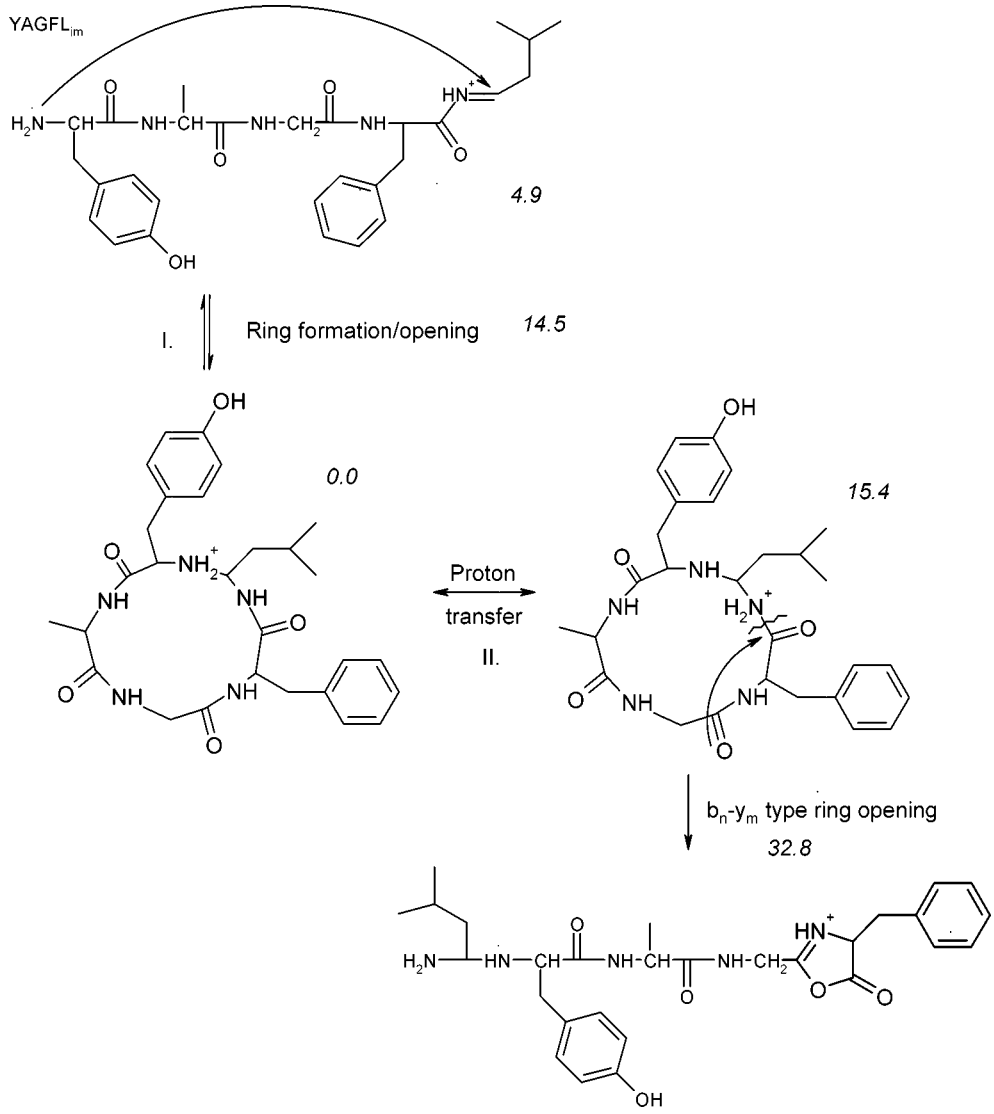

[a] After proton transfer, this structure can open up on b_n-y_m-like pathways. One of these possibilities is presented for the F−L amide bond. Relative energies (kcal mol^{-1}) are given in italics for the minima and cyclization TSs.

the b_5 ions derived from the above peptides leads to the same cyclic peptide, the dissociation of which determines the fragmentation pattern observed.

(3) The *b*-type scrambling pathways can lead to complete loss of the original sequence information, as shown for the b_5 ion of $FLYAG\text{-}NH_2$. The related chemistry is likely to be one of the reasons for false peptide identification based on MS^2 spectra that contain abundant nondirect sequence ions. Extreme care must be exercised, in particular if MS^3 spectra are used to sequence peptides. In this case, the spectrum can be dominated by nondirect sequence ions if *b* fragments are chosen for CID.

(4) Primary fragmentation of protonated *cyclo*-(YAGFL) results in loss of CO (−28 u) and of both CO and NH_3 (−45 u). Opening of the macro-ring is most favored at the A−Y amide bond to form the $AGFLY_{oxa}$ linear oxazolone and its subsequent degradation products. Ring opening at the Y−L amide bond (to form $YAGFL_{oxa}$) is more favored than ring opening at the L−F (to form $LYAGF_{oxa}$) or G−A (to form $GFLYA_{oxa}$) amide bonds. Cleavage of the F−G amide bond (to form $FLYAG_{oxa}$) seems to be completely inhibited.

(5) Protonated *cyclo*-(YAGFL) is energetically more favored than any of the linear oxazolone isomers one could derive from it. Our calculations indicate that opening of the macro-ring is energetically most favored at the A−Y amide bond, in good agreement with our experimental results. Typically, the ring-opening TSs are in a narrow internal energy range of 25−30 kcal mol^{-1}. Ring opening at the F−G amide bond is indicated to be least favored, in agreement with experimental data. Our computational data suggest that ring openings at the Y−L and L−F bonds are equally preferred.

(6) CID of the a_5 ion of $YAGFL\text{-}NH_2$ and its isomers leads to abundant nondirect sequence ions. However, most of these fragments can be assigned by assuming a reaction pattern that includes *b*-type scrambling and $a_n \rightarrow a_n$*-type rearrangement pathways. The former must be considered because *a* ions are primarily formed from *b* fragments under low-energy CID conditions. Most importantly, the fragmentation pattern of the $[MH - CO]^+$ ion of *cyclo*-(YAGFL) can be nearly completely explained without considering *a*-type scrambling pathways.

Scheme 6. Vachet−Glish Mechanism for the $a_n \rightarrow a_n^*$ Ammonia Loss Pathway of $YAGFL_{im}$[a]

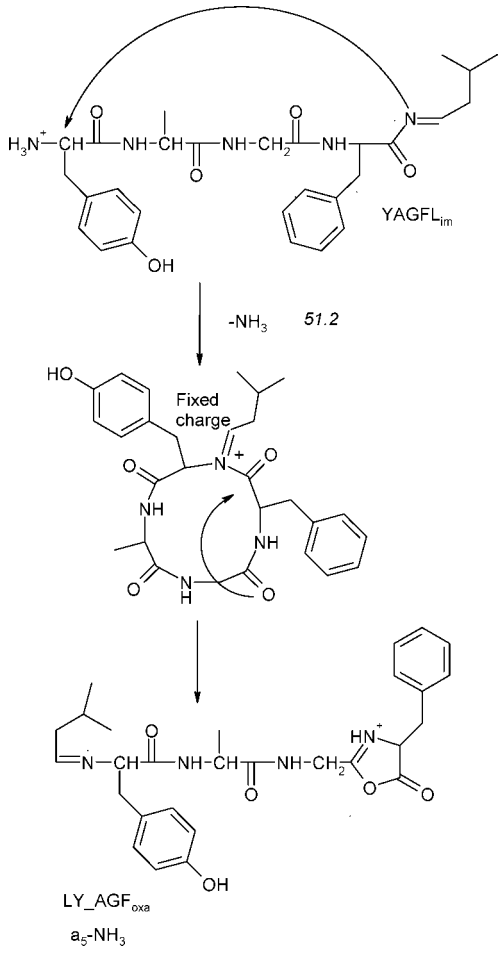

[a] S_N2-type nucleophilic attack of the C-terminal imine N on the α-carbon of Y leads to elimination of NH_3 and formation of a macrocycle. This contains a fixed charge and therefore can open up at the adjacent amide bond to form LY_AGF_{oxa}. The relative energy (kcal mol^{-1}) of the cyclization TS is given in italics.

Scheme 7. PBD Mechanism for the $a_n \rightarrow a_n^*$ Ammonia Loss Pathway of $YAGFL_{im}$[a]

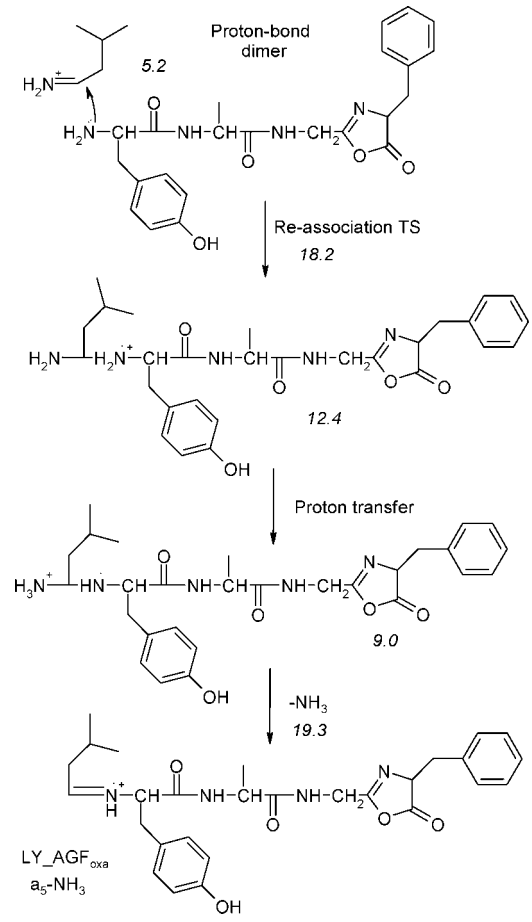

[a] The oxazolone and L imine formed on the $a_5 \rightarrow b_4$ pathway (Scheme 4) reassociate to form a rearranged isomer of $YAGFL_{im}$ that is terminated by the CHR═N−CHR′ and oxazolone groups at its termini. Proton transfer to the N-terminal amino group and subsequent ammonia loss lead to formation of LY_AGF_{oxa}. Relative energies (kcal mol^{-1}) are given in italics for the minima and various TSs.

(7) The cyclic isomers of $YAGFL_{im}$, $AGFLY_{im}$, and $LYAGF_{im}$ are energetically more favored than the linear forms. The barrier to ring opening of the cyclic form at the secondary amine group is much lower than the barrier for opening the macro-ring at an amide bond. This means that cyclic *a* isomers tend to open up at the secondary amine group, so this reaction recovers the original linear isomer. In other words, *a*-type scrambling is not favored because of the associated high barriers. This theoretical finding lends strong support to our suggested reaction scheme for *a* ions that considers only *b*-type scrambling and $a_n \rightarrow a_n^*$-type rearrangement pathways.

(8) Theoretical data suggest that the $a_n \rightarrow a_n^*$-type rearrangement does not proceed according to the mechanism originally proposed by Glish and co-workers,[14] because the corresponding ammonia elimination step involves a high barrier. Instead, elimination of the C-terminal imine via formation of a new oxazolone C-terminus occurs. The fragments are held together in proton-bound dimers that are energetically nearly as favorable as the parent a_5 ion. In this long-lived postreaction complex, the fragments can reassociate to form another a_5 isomer that bears the $NH_2-CHR-NH_2^+-CHR-$ N-terminus. Proton transfer to form $NH_3^+-CHR-NH-CHR-$ and loss of ammonia leads to the $CHR{=}NH^+-CHR-$ moiety. This PDB $a_n \rightarrow a_n^*$ mechanism is energetically much more favored than the mechanism proposed by Glish and co-workers[14] and is likely to be the major source of a^* ions and their fragments. Further atomistic details of these mechanisms are currently being investigated in our laboratories using isotope labeling. Our results there confirm the theoretical prediction described above and have been published elsewhere.[26]

(9) The experimental and computational results presented here demonstrate that rearrangement and scrambling reactions could occur for various peptide fragments. Further fragmentation of the rearranged structures leads to fragments with *m/z* values that could not be derived from the initial amino acid sequence assuming typical fragmentation pathways. Since current sequencing programs do not consider the related chemistries, product-ion spectra that are rich in nondirect sequence ions are likely to be misassigned. To assess the relevance of the rearrangement and scrambling chemistries for routine peptide sequencing, further fundamental and statistical studies are needed. Ongoing work in

(26) Bythell, B.; Molesworth, S.; Osburn, S.; Cooper, T.; Paizs, B.; Van Stipdonk, M. *J. Am. Soc. Mass Spectrom.* [Online early access]. DOI: 10.1016/j.jasms.2008.08.010. Published online: Aug 19, 2008.

our laboratories involves the synthesis and MS/MS investigation of a large number of peptides and careful statistical analysis of publicly available databases of validated peptide product-ion spectra. The corresponding results will be published elsewhere.

Acknowledgment. This work was financially supported by the NSERC Canada (A.G.H.) and the DFG (S.S., SU 244/3-1). Work by M.V.S. and S.O. was supported by U.S. National Science Foundation Grant CAREER-0239800. Funds for the purchase of the ESI-MS instrumentation were provided by the Kansas NSF-EPSCoR Program and Wichita State University. S.O. acknowledges the Fairmount College of Liberal Arts and Sciences at Wichita State University for support of her undergraduate research. C.B. is grateful for a Ph.D. fellowship from the German Cancer Research Center (DKFZ). B.P. and S.S. are grateful for financial support from the Landesstiftung Baden-Württemberg (P-CS-Prot/57). The authors thank Dr. Benjamin Bythell for critical reading of the manuscript.

Supporting Information Available: Figures S1−S6, Tables S1 and S2, and complete refs 22 and 23. This material is available free of charge via the Internet at http://pubs.acs.org.

JA805074D